Test-retest analysis of multiple ^{31}P magnetization exchange pathways using asymmetric adiabatic inversion

short title: ^{31}P inversion transfer using asymmetric adiabatic inversion

Bertrand Pouymayou[1,2], Tania Buehler[1], Roland Kreis[1], Chris Boesch[1]

[1]Dept. Clinical Research and Dept. Radiology, University of Bern, Switzerland

[2] Graduate School for Cellular and Biomedical Sciences, University of Bern, Bern, Switzerland

Corresponding author:

Chris Boesch

University Bern, AMSM (DKF/DIPR)

Pavilion 52A Inselspital, CH-3010 Bern, Switzerland

e-mail: chris.boesch@insel.ch

phone: ++41-31-632-81-74

Word count = 2798, Tables = 1, Figures = 4

Supported by the Swiss National Science Foundation #310030_149779 to CB and #320030_156952 to RK

ABSTRACT

Purpose

A ^{31}P-MR inversion transfer method (IT) with a short adiabatic inversion pulse is proposed and its test-retest reliability was evaluated for two spectral fitting strategies.

Methods

Assessment in a test-retest design (3 Tesla, vastus muscles, 12 healthy volunteers, 14 inversion times, 22ms asymmetric adiabatic inversion pulse, adiabatic excitation); spectral fitting in FitAID and jMRUI; least squares solution of the Bloch–McConnell–Solomon matrix formalism including all 14 measured time-points with equal weighting.

Results

The cohort averages of $k[PCr \rightarrow \gamma\text{-}ATP]$ are 0.246±0.050s^{-1} vs. 0.254±0.050s^{-1}, and $k[Pi \rightarrow \gamma\text{-}ATP]$ 0.086±0.033s^{-1} vs. 0.066±0.034s^{-1} (average±standard deviation, jMRUI vs. FitAID). Coefficients of variation of the differences between test and retest are lowest (9.5%) for $k[PCr \rightarrow \gamma\text{-}ATP]$ fitted in FitAID, larger (15.2%) for the fit in jMRUI, and considerably larger for $k[Pi \rightarrow \gamma\text{-}ATP]$ fitted in FitAID (43.4%) or jMRUI (47.9%). The beginning of the IT effect can be observed with magnetizations above 92% for non-inverted lines while inversion of the ATP resonances is better than -72%.

Conclusion

The performance of the asymmetric adiabatic pulse allows an accurate observation of IT effects even in the early phase; the least squares fit of the Bloch–McConnell–Solomon matrix formalism is robust; and the type of spectral fitting can influence the results significantly.

Keywords: ^{31}P MRS; inversion transfer; ATP synthesis; creatine kinase; skeletal muscle

ABBREVIATIONS

ADP	adenosine diphosphate
ATP	adenosine triphosphate (α–, β–, γ–)
B_1	radio frequency field produced by the radio frequency coil
BMI	body mass index
CK	creatine kinase
CRMVB	Cramer Rao Minimum Variance Bounds
CV	coefficient of variation
FID	free induction decay
IT	inversion transfer
jMRUI	Java Magnetic Resonance User Interface
k_{AB}	exchange rate constant of pool A > pool B (other indices accordingly)
MATLAB	matrix laboratory, a high-performance language for technical computing
MRS	magnetic resonance spectroscopy
MT	magnetization transfer
$M_{zA}(t)$	longitudinal magnetization of pool A at time t (other pools accordingly)
M_{zA}^0	equilibrium longitudinal magnetization of pool A (other pools accordingly)
NADH	nicotinamide adenine dinucleotide
NOE_{DE}	Nuclear Overhauser Effect from pool D to E (other indices accordingly)
PCr	phosphocreatine
Pi	inorganic phosphate
[Pi]	concentration of inorganic phosphate
$R_{1,A}$	apparent longitudinal relaxation rate of pool A (other pools accordingly) in the presence of magnetization transfer
SNR	signal-to-noise-ratio
T_1	longitudinal relaxation time
$T_{1,A}$	longitudinal relaxation time of pool A (other pools accordingly)
T_2	transverse relaxation time
TI	inversion time
TR	repetition time

INTRODUCTION

Magnetization transfer in ^{31}P-MR spectroscopy (^{31}P-MT) is a non-invasive method to determine biochemical reaction constants in-vivo (1,2). The majority of ^{31}P-MT experiments use saturation transfer methods (^{31}P-ST) with long selective saturation pulses to measure ATP synthesis (Pi$\rightarrow\gamma$-ATP) and the creatine kinase reaction (PCr$\rightarrow\gamma$-ATP) separately. As an alternative to ST, inversion transfer (IT) techniques introduce a perturbation of the equilibrium magnetization by an inversion of one or more resonances using short pulses. This prevents potential transfer of saturation from very small metabolite pools (3) and also offers a simultaneous determination of multiple reactions with one type of experiment.

While the interpretation of ^{31}P-MT findings is generally discussed (3-9), ST and IT shed light on different aspects and could be combined in the same subjects to study the underlying mechanisms. However, a back-to-back application of ST and IT is time-consuming and in particular IT has still the potential to be improved as shown by an increasing number of publications (10-23).

Our motivation for this study was to improve IT experiments on three levels: 1) data acquisition (shortened inversion pulse to better observe the initial MT phase), 2) spectral fitting (simultaneous fit of all spectra), 3) mathematical modeling of the time-evolution (statistically correct treatment of the noise in all spectra).

A short asymmetric adiabatic pulse (24) enables the inversion of a part of the spectrum, e.g. of all ATP resonances without affecting PCr and Pi. This approach is similar to a pioneering publication at 7T (22); however, our study differs in three aspects: (i) the transition of the inverting pulse is placed such that PCr is not inverted; (ii) a shorter pulse of 22 ms duration is used, and (iii) all measured points with identical signal-to-noise-ratio (SNR) are

included in the least squares fit of the Bloch–McConnell–Solomon matrix equations while the equilibrium signal was used for normalization of all spectra in reference (22).

Small MT effects require accurate spectral fitting of the time series, in particular at 3T with limited SNR. Since the popular jMRUI software (25,26) does not allow for simultaneous fitting of multiple spectra, the potential benefits of an alternative package ("Fitting Tool for Interrelated Arrays of Datasets, FiTAID") (27) optimized for multi-dimensional fitting, was explored.

MT effects in multiple reactions can be described in a matrix notation of the Bloch–McConnell- (18,28) or Bloch–McConnell–Solomon-equations (21). Using a least squares fit of the matrix equations leads to a simultaneous estimation of all parameters.

We evaluate the short pulse, fitting strategies, and simultaneous solution Bloch–McConnell–Solomon-equations in a test-retest design at 3 Tesla in 12 subjects and determine the coefficient of variation for the different approaches.

METHODS

The proposed IT sequence consists of an adiabatic asymmetric inversion pulse (22 ms) (24), a tunable inversion time (*TI* between 0.1ms and 19500ms), an adiabatic excitation pulse (hyperbolic secant, 2.56 ms), followed by crusher gradients. All experiments were conducted on a 3T MR system (VERIO, SIEMENS, Germany) with a double-tuned $^{1}H/^{31}P$ flexible surface coil (^{31}P coil diameter 11 cm, Rapid Biomedical, Germany). A work-in-progress field mapping sequence (CV-shim-452, SIEMENS, Erlangen/Germany) was used for shimming.

Phantom studies

The performance of the adiabatic inversion pulse was evaluated (*TR*=5s, 2 averages, 2 preparation scans) on a home-made phantom with 30mmol/l phosphate, 13mmol/l phenyl-phosphate, 0.9% NaCl, and 10% AGAR (SIGMA Aldrich, Switzerland). The delay *TI* was set to its minimum and the carrier frequency offset swept from 0 to ±100Hz with intervals of 5Hz, from ±100 to ±505Hz with intervals of 15Hz, and from ±505 to ±1555Hz with intervals of 50Hz (137 points, Fig.1).

Human studies

The sequence was applied on the right thigh muscles at rest in 12 healthy volunteers (6 males, 6 females, age 35.3±13.3 y, BMI 23.7±2.8 kg/m^2). Spectra from volunteers in two additional sessions were discarded due to hardware problems with the shim amplifier. The subjects were positioned feet-first and supine and the inferior edge of the coil was placed approximately 5 cm above the knee. Before each experiment the offset frequency of the pulse was adjusted to make sure that the inversion transition falls 60Hz upfield from the

PCr resonance (Fig.1). The IT experiment was performed twice in a test-retest design with a 10 min break while the subject left the scanner room and was repositioned (total examination time 42 min, 14 *TI* between 0.1ms and 19500ms, 8 averages, 1 preparation scan, repetition time *TR* 20s). Informed consent was obtained from all volunteers and the study was approved by the Cantonal Ethical Committee.

Data processing, fitting of spectra

The signal intensities of Pi, PCr, γ-ATP, α-ATP, and β-ATP were estimated using two different strategies (jMRUI and FitAID). Before fitting, the spectra were phased in jMRUI (0^{th} order visually; 1^{st} order with an experimentally determined 1ms delay).

In the first approach each of the 14 acquired spectra was fitted separately using jMRUI (AMARES (25,26) with truncation of 1^{st} point to avoid a baseline offset, and weighting of the 10 following points by a quarter sine-wave). Since jMRUI describes inverted resonances by a 180° phase-shift, inverted (<-60Hz) and non-inverted (>-60Hz) regions of the spectra were fitted separately. Peak area, frequency offset and linewidth were fitted with constraints depending on the resonance: the frequency offset of PCr was free, Pi was restricted to a range of 220-270Hz; all other resonances were fixed relative to PCr. All areas were free except for ATP within the multiplet structures. Except for NADH, no additional resonances (ADP etc.) were included in the model. The Lorentzian linewidths were free for PCr, limited by soft constraints for Pi (0-50Hz), and constrained to share the same linewidths for the ATP resonances.

A second fit was performed in FitAID (27) which allows for a combined fit of all 14 spectra (truncation of three first points without weighting). All areas were free and only constrained within multiplet structures. In contrast to jMRUI where either Lorentzian line or Gaussian

line shapes are available, FitAID allows also for a combination of Lorentzian and Gaussian line shapes, i.e. Voigt lines. The Lorentzian term in the Voigt line was estimated separately for each resonance but enforced not to change in time, whereas the Gaussian term was constrained to be the same for all resonances and allowed to vary through time to account for variations of the field homogeneity due to subject motion. A common phase was also assumed to be identical throughout the scans. Common frequency offsets were allowed for all peaks except for the Pi peak, which could vary due to potential pH shifts.

To judge the benefit of simultaneous fitting of all spectra in FiTAID, the Cramer Rao Minimum Variance Bounds (CRMVB) with and without simultaneous fitting were evaluated and compared to the variances found in the repeated exams.

Inversion transfer and fitting of kinetic parameters

^{31}P-MT can be described by 5 Bloch equations for the Z-magnetization of (A) Pi, (B) PCr, (C) γ-ATP, (D) α-ATP, and (E) β-ATP including terms for the Pi$\rightarrow\gamma$-*ATP* exchange (k_{AC} and k_{CA}), PCr$\rightarrow\gamma$-*ATP* exchange (k_{BC} and k_{CB}), and NOE's within the ATP molecule (NOE_{DE}, NOE_{ED}, NOE_{CE}, and NOE_{EC}). This formalism is very similar to published studies (21,22); however, without the "normalization" which has to assume infinite accuracy of the (measured) equilibrium magnetization in the divisor:

$$\frac{\partial M_{zA}(t)}{\partial t} = \frac{M_{zA}{}^{0} - M_{zA}(t)}{T_{1A}} - k_{AC} \cdot M_{zA}(t) + k_{CA} \cdot M_{zC}(t) \qquad [1]$$

$$\frac{\partial M_{zB}(t)}{\partial t} = \frac{M_{zB}{}^{0} - M_{zB}(t)}{T_{1B}} - k_{BC} \cdot M_{zB}(t) + k_{CB} \cdot M_{zC}(t) \qquad [2]$$

$$\frac{\partial M_{zC}(t)}{\partial t} = \frac{M_{zC}{}^{0} - M_{zC}(t)}{T_{1C}} - k_{CA} \cdot M_{zC}(t) + k_{AC} \cdot M_{zA}(t) \qquad [3]$$
$$- k_{CB} \cdot M_{zC}(t) + k_{BC} \cdot M_{zB}(t) - NOE_{EC} \cdot (M_{zE}{}^{0} - M_{zE}(t))$$

$$\frac{\partial M_{zD}(t)}{\partial t} = \frac{M_{zD}^{0} - M_{zD}(t)}{T_{1D}} + NOE_{ED} \cdot (M_{zE}(t) - M_{zE}(t)) \quad [4]$$

$$\frac{\partial M_{zE}(t)}{\partial t} = \frac{M_{zE}^{0} - M_{zE}(t)}{T_{1E}} - NOE_{CE} \cdot (M_{zC}^{0} - M_{zC}(t)) - NOE_{DE} \cdot (M_{zD}^{o} - M_{zD}(t)) \quad [5]$$

In matrix notation, this can be written as:

$$M_{z}(t) = M_{z}^{0} - e^{Pt} \cdot (M_{z}^{0} - M_{z}(t=0)) \quad [6]$$

with (vectors transposed for printing):

$$M_{z}(t) = \left[M_{zA}(t) \cdot\cdot M_{zB}(t) \cdot\cdot M_{zC}(t) \cdot\cdot M_{zD}(t) \cdot\cdot M_{zE}(t)\right]' \quad [7]$$

$$M_{z}^{0} = \left[M_{zA}^{0} \cdot\cdot M_{zB}^{0} \cdot\cdot M_{zC}^{0} \cdot\cdot M_{zD}^{0} \cdot\cdot M_{zE}^{0}\right]' \quad [8]$$

$$P = \begin{bmatrix} -R_{1,A} & 0 & k_{CA} & 0 & 0 \\ 0 & -R_{1,B} & k_{CB} & 0 & 0 \\ k_{AC} & k_{BC} & -R_{1,C} & 0 & NOE_{EC} \\ 0 & 0 & 0 & -R_{1,D} & NOE_{ED} \\ 0 & 0 & NOE_{CE} & NOE_{DE} & -R_{1,E} \end{bmatrix} \quad [9]$$

$$R_{1,A} = \frac{1}{T_{1,A}} + k_{AC} \quad [10]$$

$$R_{1,B} = \frac{1}{T_{1,B}} + k_{BC} \quad [11]$$

$$R_{1,C} = \frac{1}{T_{1,C}} + k_{CA} + k_{CB} \quad [12]$$

$$R_{1,D} = \frac{1}{T_{1,D}} \quad [13]$$

$$R_{1,E} = \frac{1}{T_{1,E}} \quad [14]$$

and the values can be found by a numerical solution of the matrix equation [6].

Assuming steady-state, k_{CA} and k_{CB} were calculated from:

$$k_{CA} = k_{AC} \cdot \frac{M_{zA}^{\ 0}}{M_{zC}^{\ 0}} \quad [15]$$

$$k_{CB} = k_{BC} \cdot \frac{M_{zB}^{\ 0}}{M_{zC}^{\ 0}} \quad [16]$$

and the forward and backward NOE's were assumed to be equal:

$$NOE_{ED} = NOE_{DE} \quad [17]$$

$$NOE_{EC} = NOE_{CE} \quad [18]$$

This reduced the total of 23 independent parameters (k_{BC}, k_{CB}, k_{AC}, k_{CA}, $T_{1,A}$, $T_{1,B}$, $T_{1,C}$, $T_{1,D}$, $T_{1,E}$, M_{zA}^{0}, M_{zB}^{0}, M_{zC}^{0}, M_{zD}^{0}, M_{zE}^{0}, $M_{zA}(0)$, $M_{zB}(0)$, $M_{zC}(0)$, $M_{zD}(0)$, $M_{zE}(0)$, NOE_{DE}, NOE_{CE}, NOE_{ED}, NOE_{EC}) of the equation system [6] to 19 which were determined simultaneously by the least squares fitting "lsqcurvefit" in MATLAB (R2011b, MathWorks Inc., Natick MA, USA).

Statistics

Statistical illustrations (Coefficient of Variation, Bland-Altman plot) were calculated in EXCEL 2007 (Microsoft, Redmond WA, USA).

RESULTS

Pulse characteristics *in-vitro*

In a phantom, the characteristics of the inversion pulse were determined over the whole spectral range (Fig.1). If the excitations at the chemical shift positions in vivo are compared, PCr is slightly reduced relative to Pi and the ATP-resonances are inverted incompletely; however, the transition between PCr and γ-ATP is small enough to bring the two adjacent resonances PCr and γ-ATP into the desired states.

Time development *in-vivo*

Figure 2 illustrates a typical fit of the time development of Pi, PCr, γ-ATP, α-ATP, and β-ATP. The ratio of the fitted values of $M_Z(0)/M_Z^0$, i.e. the ratio of magnetizations at the very beginning and the very end of the transfer are listed in Table 1. The starting values $M_Z(0)/M_Z^0$ for Pi and PCr are comparable in the jMRUI analysis (avg±sd 92.3%±7.7% and 92.8%±1.6%) and even slightly better in the FitAID analysis (96.6%±2.9% and 94.6%±1.6%). The inversion of the ATP resonances was between -72.4% and -78.5% for the jMRUI analysis with similar results from FitAID (-75.0% to -82.1%).

Test-retest of the parameter fits

Table 1 and Figures 3 and 4 show the least squares solution of matrix [7] based on spectral fits from jMRUI and FitAID, respectively. The group averages of *k[PCr→γ-ATP]* and *k[Pi→γ-ATP]* are similar for the two fitting strategies. CV's of the differences between test and retest are lowest (9.5%) for *k[PCr→γ-ATP]* fitted in FitAID, larger (15.2%) for the fit in jMRUI, and considerably larger for *k[Pi→γ-ATP]* fitted in FitAID (43.4%) or jMRUI (47.9%). It is obvious that parameters which are strongly dependent on the behavior of PCr (e.g.

k[PCr→γ-ATP], *T1* of PCr, or the MT-influenced recovery-curve of γ-ATP) are better defined, i.e. result in a lower CV than parameters with little dependence on this large signal (e.g. *T1* and NOE of α- and β-ATP). In general, the ratios of amplitudes ($M_Z(0)/M_Z^0$) which describe the pulse behavior are defined with CV's well below 10%.

Influence of the spectral fitting algorithms

The two fitting strategies agree very well for *k[PCr→γ-ATP]* (0.246±0.050s^{-1} vs. 0.254±0.050s^{-1}, avg±sd, jMRUI vs. FitAID), which is primarily determined by the strong signal of PCr; however, there is a considerable difference for *k[→γ-ATP]* (0.086±0.033s^{-1} vs. 0.066±0.034s^{-1}) between the two algorithms (Table 1).

The CRMVB for the Pi area parameter was found to be about 41% higher if individual spectra were fitted compared to fitting the series as a whole. In addition, the CV between the Pi-amplitudes in repeated exams (4.1%) was very similar to the CV expected based on CRMVB (3.6%), confirming that the SNR was limiting the precision of the Pi evaluation.

DISCUSSION

This test-retest study had 3 distinct targets:

(1) The evaluation of a relatively short (22ms) adiabatic inversion pulse allowing observation of the IT early after initiation.

(2) Evaluation of a least-squares solution of the Bloch–McConnell–Solomon matrix formalism which includes all error-prone M(t) measurements in the fitting algorithm with the correct weighting.

(3) Evaluation of the influence of two spectral fitting algorithms (jMRUI vs. FitAID) that differ in their capabilities for simultaneous fitting of multiple spectra.

Pulse performance and early time-evolution

The pulse used in this study (24) is similar to the one used by Ren et al. (22) at 7 Tesla, however, the shorter duration (22 vs. 42ms) allows for earlier observation of the IT effect and reduces relaxation during the pulse (29,30). The $M_Z(0)/M_Z^0$ ratios (Table 1) of >92% for Pi and PCr help to define the time-evolution at an early phase. This part of the curve is particularly important for the fitting algorithm since it helps to define those parameters of the MT effect which have less influence in a later phase of the time-evolution. The pulse inverts the ATP-resonances adequately while the sharpness of the pulse transition is sufficient to leave PCr almost untouched (Table 1). A shift of the pulse transition to the left of PCr (22) amplifies the effect on Pi beneficially; however, at the costs of a considerably limited accuracy for the creatine-kinase reaction.

Determination of *k*-, T_1, and NOE-values

The test-retest accuracy of the creatine kinase reaction constant *k[PCr→γ-ATP]* yields excellent CV's and the measured values are well in the range of published literature (21,22,31-35). In turn, the small Pi resonance defines the signal development less accurately for *k[Pi→γ-ATP],* resulting in a much larger variance; however, the average cohort values are well in the range of published literature (4,7,20-23,33,34). For the determination of *k[Pi→γ-ATP],* inversion of the PCr resonance (22) is beneficial; however, at the cost of limited accuracy for *k[PCr→γ-ATP]*.

The number of 19 fitted parameters seems large; however, 70 data points are available to fit 19 parameters (5 resonances measured 14 times). In particular, we include the measured value M(19500 ms) in the fit. A reduction of the number of parameters by a "normalization" (22) $m_z(t)$ = M(t)/M(equilibrium) would require an infinitely accurate measured M(equilibrium). Otherwise, this "normalization" propagates the measurement error of M(equilibrium) to all fitted values and leads to bias since the fitting algorithm assumes m_z(t->equilibrium)=1. Including the measured M(19500 ms) in our fitting algorithm treats all error-prone measurements equally without a bias for M(equilibrium).

T1 values determined in this study were perfectly in line with literature values at 3T for PCr (36,37), yet considerably smaller than those published for the ATP resonances and larger than those published for Pi. The major reason for the discrepancy might be the different types of measurements (IT vs. inversion/saturation recovery only) which weight interfering effects like MT, NOE, summation over different pools etc. differently.

Influence of fitting strategies

The differences between *k[PCr→γ-ATP]* and *k[Pi→γ-ATP]* as well as the comparison of the $M_Z(0)/M_Z^0$ ratios show that the results agree well between jMRUI and FitAID for peaks

with excellent SNR. However, the differences become larger if the resonances are smaller (e.g. Pi) and/or go through zero during the recovery process (i.e. γ-, α-, β-ATP). The differences can mainly be explained by the different handling of prior knowledge over multiple spectra by FitAID as compared to jMRUI. Specifically, the variance of the fitted Pi peak area was found to be 41% higher if the 14 spectra were fitted individually as compared to simultaneously (both CRMVB determined in FiTAID to prevent bias based on other differences in the programs or the other differences in fitting models). In addition, the two fitting algorithms have also other differences that might influence the fitting accuracy, e.g. FiTAID allows for a use of Voigt lines and thus a fixation of the T_2 decay while the shimming variation can be considered in the Gaussian term. We conclude that a fitting approach with simultaneous treatment of a time series (in our approach FiTAID) is clearly more robust than an individual spectrum fit approach.

Limitations:

The study has limitations; in particular that the fit of Pi in jMRUI was not very robust. Even though one expects that the fit would become more stable after the introduction of additional prior knowledge, we found in our approach that the algorithm seemed to get trapped in local minima more often if prior knowledge was enforced, resulting in obvious outliers (e.g. zero amplitude for a clearly visible Pi etc.). Increased SNR (more acquisitions, higher field strength, optimized coils) could have improved it. The study was performed at 3T while the higher SNR at 7T has been shown to promote excellent results (20-22,34,35). Since most clinical systems are at 3T, the presented data is nonetheless relevant for clinical sites. Two compartments with different pH and *T1* can be distinguished at higher field strength (38); however, this differentiation was not included in the presented formalism

since one of the compartments is only about 10% of the total signal and thus hardly quantifiable at 3T. Only the resonances of ATP are in the model while ADP and other nucleotides are omitted since we expect that their contributions are small and not determinable with sufficient precision. Only healthy volunteers have been enrolled, yielding an estimation of the measurement error; however, inclusion of patients or subjects with different training status will be needed to estimate effect sizes in subsequent power analyses. Several extensions and improvements of the study design can be envisioned, e.g. shortening of the very long *TR* or to shift the inversion pulse to include different resonances.

Conclusions

The suggested adiabatic asymmetric inversion pulse is short enough to observe the effect of magnetization inversion early on, while the pulse performance (inversion, transition bandwidth) is still very good. The reaction rates $k[PCr \rightarrow \gamma\text{-}ATP]$ can be determined with a CV of <10% (FitAID) while $k[Pi \rightarrow \gamma\text{-}ATP]$ suffers from the lower SNR of Pi, resulting in a CV of >40%. The least squares fit of the matrix description is robust; however, only those parameters that influence the shape of M(t) of major resonances significantly show a low CV. The simultaneous fit of all spectra in FitAID leads to smaller CV's for the kinetic constants than independent spectral fits for all spectra in jMRUI.

Acknowledgements

This work was supported by the Swiss National Science Foundation (SNF Grant #310030-149779 to CB and #320030_156952 to RK). We want to express our particular thank to the anonymous reviewer of our recent article (23), who triggered this study with a very insightful comment.

REFERENCES

1. Forsen S, Hoffman RA. Study of Moderately Rapid Chemical Exchange Reactions by Means of Nuclear Magnetic Double Resonance. J Chem Phys 1963;39:2892-2901.

2. De Graaf RA. In-vivo NMR spectroscopy : Principles and techniques. 2 ed. Chichester UK: John Wiley & Sons; 2007.

3. Balaban RS, Koretsky AP. Interpretation of 31P NMR saturation transfer experiments: what you can't see might confuse you. Focus on "Standard magnetic resonance-based measurements of the Pi-->ATP rate do not index the rate of oxidative phosphorylation in cardiac and skeletal muscles. Am J Physiol 2011;301:C12-C15.

4. Kemp GJ. The interpretation of abnormal P-31 magnetic resonance saturation transfer measurements of P-i/ATP exchange in insulin-resistant skeletal muscle. Am J Physiol 2008;294:E640-E642.

5. Kemp GJ, Brindle KM. What Do Magnetic Resonance-Based Measurements of Pi->ATP Flux Tell Us About Skeletal Muscle Metabolism? Diabetes 2012;61:1927-1934.

6. From AH, Ugurbil K. Standard magnetic resonance-based measurements of the Pi-->ATP rate do not index the rate of oxidative phosphorylation in cardiac and skeletal muscles. Am J Physiol 2011;301:C1-C11.

7. Schmid AI, Schrauwen-Hinderling VB, Andreas M, Wolzt M, Moser E, Roden M. Comparison of measuring energy metabolism by different (31) P-magnetic resonance spectroscopy techniques in resting, ischemic, and exercising muscle. Magn Reson Med 2012;67:898-905.

8. van den Broek NM, Ciapaite J, Nicolay K, Prompers JJ. Comparison of in-vivo postexercise phosphocreatine recovery and resting ATP synthesis flux for the assessment of skeletal muscle mitochondrial function. Am J Physiol 2010;299:C1136-C1143.

9. Nabuurs C, Huijbregts B, Wieringa B, Hilbers CW, Heerschap A. 31P saturation transfer spectroscopy predicts differential intracellular macromolecular association of ATP and ADP in skeletal muscle. J Biol Chem 2010;285:39588-39596.

10. Alger JR, Prestegard JH. Investigation of Peptide-Bond Isomerization by Magnetization Transfer NMR. J Magn Reson 1977;27:137-141.

11. Brown TR, Ogawa S. 31P nuclear magnetic resonance kinetic measurements on adenylatekinase. Proc Natl Acad Sci USA 1977;74:3627-3631.

12. Meyer RA, Kushmerick MJ, Brown TR. Application of 31P-NMR spectroscopy to the study of striated muscle metabolism. Am J Physiol 1982;242:C1-C11.

13. Degani H, Alger JR, Shulman RG, Petroff OA, Prichard JW. 31P magnetization transfer studies of creatine kinase kinetics in living rabbit brain. Magn Reson Med 1987;5:1-12.

14. Hsieh PS, Balaban RS. Saturation and inversion transfer studies of creatine kinase kinetics in rabbit skeletal muscle in-vivo. Magn Reson Med 1988;7:56-64.

15. McFarland EW, Kushmerick MJ, Moerland TS. Activity of creatine kinase in a contracting mammalian muscle of uniform fiber type. Biophys J 1994;67:1912-1924.

16. Mora BN, Narasimhan PT, Ross BD. 31P magnetization transfer studies in the monkey brain. Magn Reson Med 1992;26:100-115.

17. Haseler LJ, Brooks WM, Irving MG, Bulliman BT, Kuchel PW, Doddrell DM. Use of inversion spin transfer to monitor creatine kinase kinetics in rat skeletal muscle in-vivo. Biochem Int 1986;12:613-618.

18. Joubert F, Vrezas I, Mateo P, Gillet B, Beloeil JC, Soboll S, Hoerter JA. Cardiac creatine kinase metabolite compartments revealed by NMR magnetization transfer spectroscopy and subcellular fractionation. Biochemistry 2001;40:2129-2137.

19. Joubert F, Mazet JL, Mateo P, Hoerter JA. 31P NMR detection of subcellular creatine kinase fluxes in the perfused rat heart: contractility modifies energy transfer pathways. J Biol Chem 2002;277:18469-18476.

20. Ren J, Sherry AD, Malloy CR. A simple approach to evaluate the kinetic rate constant for ATP synthesis in resting human skeletal muscle at 7 T. NMR Biomed 2015;[Epub ahead of print]:doi: 10.1002/nbm.3310.

21. Ren J, Yang B, Sherry AD, Malloy CR. Exchange kinetics by inversion transfer: Integrated analysis of the phosphorus metabolite kinetic exchanges in resting human skeletal muscle at 7 T. Magn Reson Med 2015;73:1359-1369.

22. Ren J, Sherry AD, Malloy CR. Amplification of the effects of magnetization exchange by P band inversion for measuring adenosine triphosphate synthesis rates in human skeletal muscle. Magn Reson Med 2015;74:1505-1514.

23. Buehler T, Kreis R, Boesch C. Comparison of 31P saturation and inversion magnetization transfer in human liver and skeletal muscle using a clinical MR-system and surface coils. NMR Biomed 2015;28:188-199.

24. Hwang TL, van Zijl PCM, Garwood M. Asymmetric adiabatic pulses for NH selection. J Magn Reson 1999;138:173-177.

25. Naressi A, Couturier C, Devos JM, Janssen M, Mangeat C, de Beer R, Graveron-Demilly D. Java-based graphical user interface for the MRUI quantitation package. Magn Reson Mater Phy 2001;12:141-152.

26. Vanhamme L, vandenBoogaart A, Van Huffel S. Improved method for accurate and efficient quantification of MRS data with use of prior knowledge. J Magn Reson 1997;129:35-43.

27. Chong DGQ, Kreis R, Bolliger CS, Boesch C, Slotboom J. Two-dimensional linear-combination model fitting of magnetic resonance spectra to define the macromolecule baseline using FiTAID, a Fitting Tool for Arrays of Interrelated Datasets. Magn Reson Mater Phy 2011;24:147-164.

28. Gabr RE, Weiss RG, Bottomley PA. Correcting reaction rates measured by saturation-transfer magnetic resonance spectroscopy. J Magn Reson 2008;191:248-258.

29. Norris DG. Adiabatic radiofrequency pulse forms in biomedical nuclear magnetic resonance. Concepts Magn Reson 2002;14:89-101.

30. Norris DG, Ludemann H, Leibfritz D. An Analysis of the Effects of Short T2 Values on the Hyperbolic-Secant Pulse. J Magn Reson 1991;92:94-101.

31. Bottomley PA, Ouwerkerk R, Lee RF, Weiss RG. Four-angle saturation transfer (FAST) method for measuring creatine kinase reaction rates in-vivo. Magn Reson Med 2002;47:850-863.

32. Schär M, El-Sharkawy AM, Weiss RG, Bottomley PA. Triple repetition time saturation transfer (TRiST) 31P spectroscopy for measuring human creatine kinase reaction kinetics. Magn Reson Med 2010;63:1493-1501.

33. Befroy DE, Rothman DL, Petersen KF, Shulman GI. 31P-Magnetization Transfer Magnetic Resonance Spectroscopy Measurements of In-vivo Metabolism. Diabetes 2012;61:2669-2678.

34. Valkovic L, Ukropcova B, Chmelik M, Balaz M, Bogner W, Schmid AI, Frollo I, Zemkova E, Klimes I, Ukropec J, Trattnig S, Krssak M. Interrelation of 31P-MRS metabolism measurements in resting and exercised quadriceps muscle of overweight-to-obese sedentary individuals. NMR Biomed 2013;26:1714-1722.

35. Valkovic L, Chmelik M, Just K, I, Krssak M, Gruber S, Frollo I, Trattnig S, Bogner W. Time-resolved phosphorous magnetization transfer of the human calf muscle at 3 T and 7 T: a feasibility study. Eur J Radiol 2013;82:745-751.

36. Meyerspeer M, Krssak M, Moser E. Relaxation times of 31P-metabolites in human calf muscle at 3 T. Magn Reson Med 2003;49:620-625.

37. El-Sharkawy AM, Schar M, Ouwerkerk R, Weiss RG, Bottomley PA. Quantitative cardiac 31P spectroscopy at 3 Tesla using adiabatic pulses. Magn Reson Med 2009;61:785-795.

38. Kan HE, Klomp DW, Wong CS, Boer VO, Webb AG, Luijten PR, Jeneson JA. In-vivo 31P MRS detection of an alkaline inorganic phosphate pool with short T1 in human resting skeletal muscle. NMR Biomed 2010;23:995-1000.

Table

Parameter	Unit	FitAID				jMRUI			
		Cohort		Δ(Test-Retest)		Cohort		Δ(Test-Retest)	
		Average	SD	SD	CV	Average	SD	SD	CV
k[Pi→γ-ATP]	s^{-1}	0.066	0.034	0.029	43.4%	0.086	0.033	0.041	47.9%
k[PCr→γ-ATP]	s^{-1}	0.254	0.050	0.024	9.5%	0.246	0.050	0.037	15.2%
$M_z(0)/M_z^0$ [Pi]	%	96.6	2.9	3.4	3.5%	92.3	7.7	6.7	7.3%
$M_z(0)/M_z^0$ [PCr]	%	94.6	1.6	2.2	2.3%	92.8	1.6	1.8	2.0%
$M_z(0)/M_z^0$ [γ-ATP]	%	-78.9	8.2	8.0	10.2%	-73.8	5.0	3.5	4.8%
$M_z(0)/M_z^0$ [α-ATP]	%	-82.1	3.0	3.1	3.8%	-78.5	3.3	3.1	3.9%
$M_z(0)/M_z^0$ [β-ATP]	%	-75.0	3.4	2.6	3.5%	-72.4	3.6	3.0	4.1%
T_1 [Pi]	s	8.07	5.36	4.85	60.0%	12.90	6.38	8.86	68.7%
T_1 [PCr]	s	6.76	1.20	1.63	24.1%	6.82	0.86	0.89	13.0%
T_1 [γ-ATP]	s	2.04	0.72	0.47	23.2%	2.03	0.64	0.66	32.4%
T_1 [α-ATP]	s	1.19	0.69	1.08	90.4%	0.82	0.49	0.60	72.5%
T_1 [β-ATP]	s	0.64	0.37	0.57	88.9%	0.46	0.39	0.51	110.3%
NOE [γ-ATP → β-ATP]	-	0.32	0.10	0.15	48.1%	0.37	0.10	0.156	39.4%
NOE [β-ATP → α-ATP]	-	1.00	0.69	1.06	105.5%	1.57	0.75	0.92	58.6%

Table 1 shows the results from the test-retest experiments and the coefficients of variation (CV) for the differences between test and retest for the two fitting strategies. The standard deviations (SD) from the cohort include the variations between the individual subjects while the SD from the differences only include the variations between test and retest. The CV's are calculated as SD of the differences divided by the overall average.

Figure Captions

Figure 1 (A) The pulse characteristics of the inversion pulse measured with a home-made phantom is illustrated by the resonance of PO_4 (20 Hz apodization) which is shifted by an offset of the carrier frequency in a range of ±1005 Hz. The excitation at 0ppm (chemical shift position of PCr, 87%) is slightly reduced relative to 5.0ppm (position of Pi), and the inversion at the chemical shift positions of the ATP-resonances is not complete (γ-ATP -73%, α-ATP -68%, β-ATP -55%). Of note: this reduces the signal-to-noise of the time-evolution slightly yet does not influence the ratio of *Mz(0)/Mz0* in Table 1. (B) For comparison, a series of *in-vivo* spectra is shown to illustrate the time-evolution of the spectra on one hand and the sharp transition between PCr and γ-ATP on the other hand; the transition is placed at -60 Hz from the PCr resonance.

Figure 2 Example of experimental and fitted data (jMRUI) of the IT development in one healthy volunteer. The excellent agreement between fit and experimental data is striking for PCr and the ATP resonances; however, the limited signal-to-noise of the small Pi resonance leads to considerable scattering of this data and subsequently to a less robust fit.

Figure 3 Agreement of *k[PCr→γ-ATP]* for the two spectral fitting methods between test and retest, respectively. The upper trace shows a Bland-Altman analysis between test and retest; the lower trace shows the absolute values for each volunteer.

Figure 4 Agreement of *k[Pi→γ-ATP]* for the two spectral fitting methods between test and retest, respectively. The upper trace shows a Bland-Altman analysis between test and re-test; the lower trace shows the absolute values for each volunteer.

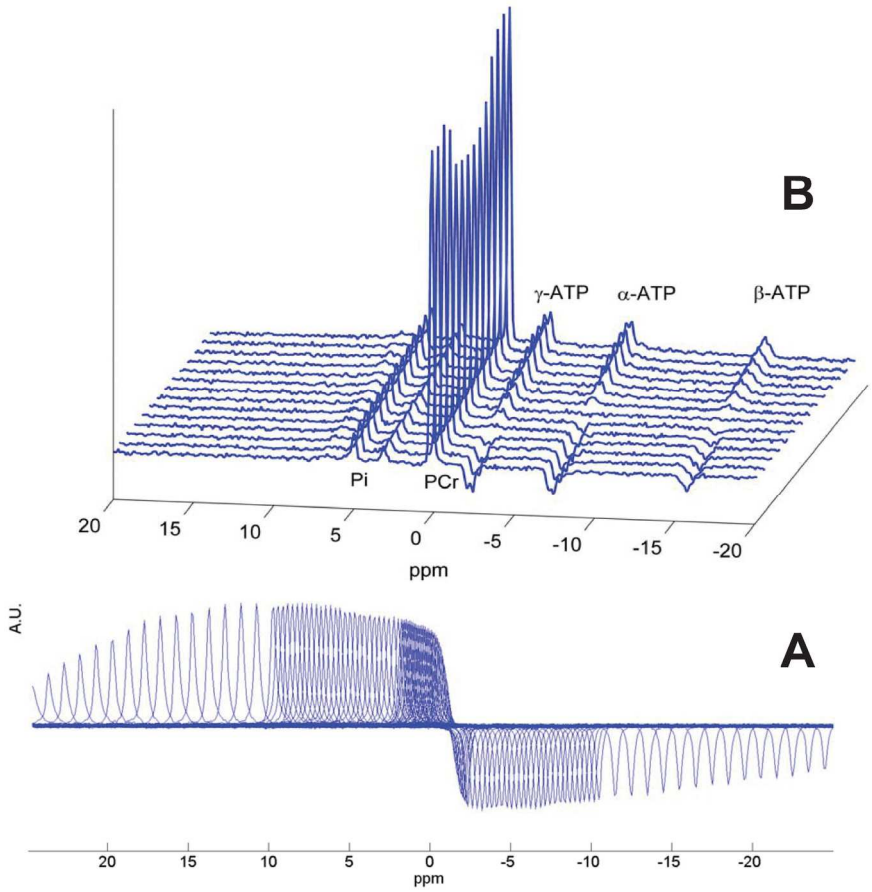

Figure 1 (A) The pulse characteristics of the inversion pulse measured with a home-made phantom is illustrated by the resonance of PO_4 (20 Hz apodization) which is shifted by an offset of the carrier frequency in a range of ±1005 Hz. The excitation at 0ppm (chemical shift position of PCr, 87%) is slightly reduced relative to 5.0ppm (position of Pi), and the inversion at the chemical shift positions of the ATP-resonances is not complete (γ-ATP -73%, α-ATP -68%, β-ATP -55%). Of note: this reduces the signal-to-noise of the time-evolution slightly yet does not influence the ratio of $M_z(0)/M_z0$ in Table 1. (B) For comparison, a series of in-vivo spectra is shown to illustrate the time-evolution of the spectra on one hand and the sharp transition between PCr and γ-ATP on the other hand; the transition is placed at -60 Hz from the PCr resonance.
185x175mm (300 x 300 DPI)

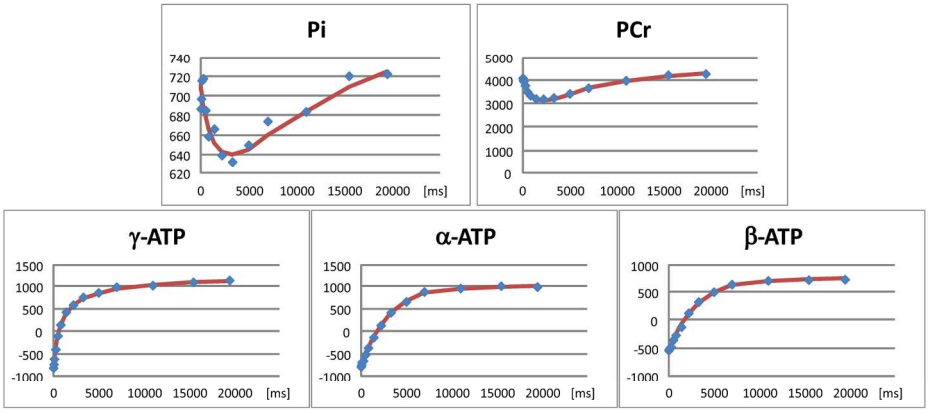

Figure 2 Example of experimental and fitted data (jMRUI) of the IT development in one healthy volunteer. The excellent agreement between fit and experimental data is striking for PCr and the ATP resonances; however, the limited signal-to-noise of the small Pi res-onance leads to considerable scattering of this data and subsequently to a less robust fit.
190x142mm (300 x 300 DPI)

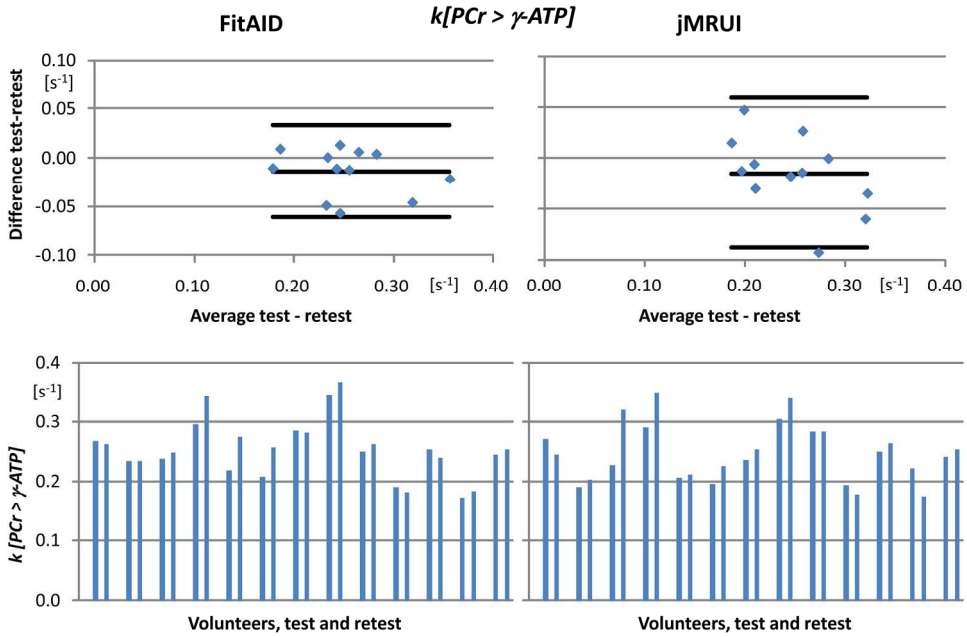

Figure 3 Agreement of *k[PCr→γ-ATP]* for the two spectral fitting methods between test and retest, respectively. The upper trace shows a Bland-Altman analysis between test and re-test; the lower trace shows the absolute values for each volunteer.
190x142mm (300 x 300 DPI)

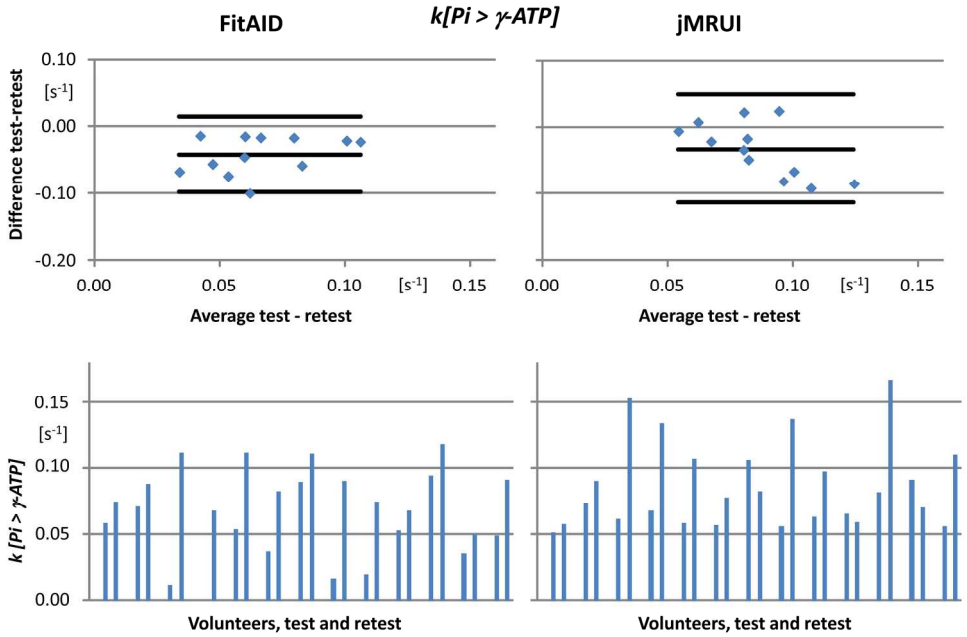

Figure 4 Agreement of *k[Pi→γ-ATP]* for the two spectral fitting methods between test and retest, respectively. The upper trace shows a Bland-Altman analysis between test and re-test; the lower trace shows the absolute values for each volunteer.
190x142mm (300 x 300 DPI)